

**AFRL-AFOSR-UK-TR-2011-0014**



## **Shock Boundary Layer Interaction Flow Control with Micro Vortex Generators**

**Holger Babinsky**

**University of Cambridge  
Engineering Department  
Trumpington Street  
Cambridge, United Kingdom CB2 1PZ**

EOARD GRANT 08-3091

May 2011

Final Report for 1 October 2008 to 31 March 2011

**Distribution Statement A: Approved for public release distribution is unlimited.**

**Air Force Research Laboratory  
Air Force Office of Scientific Research  
European Office of Aerospace Research and Development  
Unit 4515 Box 14, APO AE 09421**

**REPORT DOCUMENTATION PAGE**

Form Approved OMB No. 0704-0188

Public reporting burden for this collection of information is estimated to average 1 hour per response, including the time for reviewing instructions, searching existing data sources, gathering and maintaining the data needed, and completing and reviewing the collection of information. Send comments regarding this burden estimate or any other aspect of this collection of information, including suggestions for reducing the burden, to Department of Defense, Washington Headquarters Services, Directorate for Information Operations and Reports (0704-0188), 1215 Jefferson Davis Highway, Suite 1204, Arlington, VA 22202-4302. Respondents should be aware that notwithstanding any other provision of law, no person shall be subject to any penalty for failing to comply with a collection of information if it does not display a currently valid OMB control number.  
**PLEASE DO NOT RETURN YOUR FORM TO THE ABOVE ADDRESS.**

<b>1. REPORT DATE (DD-MM-YYYY)</b> 24-05-2011	<b>2. REPORT TYPE</b> Final Report	<b>3. DATES COVERED (From - To)</b> 1 October 2008 -31 March 2011
--	---------------------------------------	--

<b>4. TITLE AND SUBTITLE</b>  <b>Shock Boundary Layer Interaction Flow Control with Micro Vortex Generators</b>	<b>5a. CONTRACT NUMBER</b> FA8655-08-1-3091
	<b>5b. GRANT NUMBER</b> <b>Grant 08-3091</b>
	<b>5c. PROGRAM ELEMENT NUMBER</b> 61102F

<b>6. AUTHOR(S)</b>  Professor Holger Babinsky	<b>5d. PROJECT NUMBER</b>
	<b>5d. TASK NUMBER</b>
	<b>5e. WORK UNIT NUMBER</b>

<b>7. PERFORMING ORGANIZATION NAME(S) AND ADDRESS(ES)</b> University of Cambridge Engineering Department Trumpington Street Cambridge, United Kingdom CB2 1PZ	<b>8. PERFORMING ORGANIZATION REPORT NUMBER</b>  N/A
---	--

<b>9. SPONSORING/MONITORING AGENCY NAME(S) AND ADDRESS(ES)</b>  EOARD Unit 4515 BOX 14 APO AE 09421	<b>10. SPONSOR/MONITOR'S ACRONYM(S)</b> AFRL/AFOSR/RSW (EOARD)
	<b>11. SPONSOR/MONITOR'S REPORT NUMBER(S)</b>  <b>AFRL-AFOSR-UK-TR-2011-0014</b>

**12. DISTRIBUTION/AVAILABILITY STATEMENT**  
Approved for public release; distribution is unlimited.

**13. SUPPLEMENTARY NOTES**

**14. ABSTRACT**

The flow through a terminating shock-wave and subsequent subsonic diffuser typically found in supersonic inlets has been simulated using a small-scale wind tunnel. Experiments have been conducted at an inflow Mach number of 1.4 using a dual channel working section to produce a steady near-normal shock-wave. The setup was designed so that the location of the shock-wave could be varied relative to the diffuser. As the near-normal shock-wave was moved downstream and into the diffuser, an increasingly distorted, three-dimensional and separated flow was observed. Compared to the interaction of a normal shock-wave in a constant area duct, the addition of the diffuser resulted in more prominent corner interactions. A variety of control philosophies were then employed to improve pressure recovery and reduce flow distortion. When control was employed along the centre-line, improvements in this region were masked by enlarged corner separations, and even asymmetric solutions in some configurations. On the other hand, when control was applied in the corners, although separation from the corners was removed this was replaced by a more two-dimensional floor separation. Only when control of both the centre-line and corners were addressed simultaneously was an overall improvement in the pressure recovery and distortion obtained. Using an appropriate control configuration (VGs on the centre-line and bleed in the corners) a highly separated flowfield is drastically improved, leading to the conclusion that there is significant potential for the use of nonbleed supersonic control when implemented in the correct manner.

**15. SUBJECT TERMS**  
EOARD, Aerodynamics, Shock Waves, Boundary Layer Control

<b>16. SECURITY CLASSIFICATION OF:</b>			<b>17. LIMITATION OF ABSTRACT</b>  SAR	<b>18. NUMBER OF PAGES</b>  34	<b>19a. NAME OF RESPONSIBLE PERSON</b> Gregg Abate
<b>a. REPORT</b> UNCLAS	<b>b. ABSTRACT</b> UNCLAS	<b>c. THIS PAGE</b> UNCLAS			<b>19b. TELEPHONE NUMBER (Include area code)</b> +44 (0)1895 616021



# Shock Boundary Layer Interaction Flow Control with Micro Vortex Generators

1st October 2008 – 31 March 2011

Grant number: FA8655-08-1-3091

Neil Titchener and Holger Babinsky  
Department of Engineering,  
University of Cambridge,  
Trumpington St.,  
Cambridge,  
United Kingdom

# Shock Boundary Layer Interaction Flow Control with Micro Vortex Generators

Neil Titchener and Holger Babinsky

The flow through a terminating shock-wave and subsequent subsonic diffuser typically found in supersonic inlets has been simulated using a small-scale wind tunnel. Experiments have been conducted at an inflow Mach number of 1.4 using a dual channel working section to produce a steady near-normal shock-wave. The setup was designed so that the location of the shock-wave could be varied relative to the diffuser. As the near-normal shock-wave was moved downstream and into the diffuser, an increasingly distorted, three-dimensional and separated flow was observed. Compared to the interaction of a normal shock-wave in a constant area duct, the addition of the diffuser resulted in more prominent corner interactions. A variety of control philosophies were then employed to improve pressure recovery and reduce flow distortion. When control was employed along the centre-line, improvements in this region were masked by enlarged corner separations, and even asymmetric solutions in some configurations. On the other hand, when control was applied in the corners, although separation from the corners was removed this was replaced by a more two-dimensional floor separation. Only when control of both the centre-line and corners were addressed simultaneously was an overall improvement in the pressure recovery and distortion obtained. Using an appropriate control configuration (VGs on the centre-line and bleed in the corners) a highly separated flow field is drastically improved, leading to the conclusion that there is significant potential for the use of nonbleed supersonic control when implemented in the correct manner.

---

## Nomenclature

- $C_f = \tau_w / \frac{1}{2} \rho_{fs} u_{fs}^2$  = local skin-friction coefficient  
 $D = \frac{p_{02,max} - p_{02,min}}{\bar{p}_{02}}$  = flow distortion  
 $h = \mu VG$  height  
 $H_i^*$  = incompressible boundary-layer shape factor ( $\frac{\delta_i^*}{\theta_i^*}$ )  
 $p_{0i}$  = time-averaged stagnation pressure at station i  
 $p_i$  = time-averaged wall pressure at station i  
 $\bar{p}_0$  = area-averaged pressure recovery at the Pitot rake ( $\frac{\bar{p}_{02}}{p_{01}}$ )  
 $u$  = time-averaged streamwise velocity  
 $u_{fs}$  = time-averaged freestream streamwise velocity  
 $u^* = \sqrt{\frac{\tau_w}{\rho_w}}$  = wall-shear velocity  
 $w$  = tunnel half-width = 57 mm  
 $x$  = streamwise displacement relative to the diffuser entrance  
 $x_{VG}$  = position of  $\mu VG$  trailing edge  
 $\Delta x$  = distance between baseline separation and  $\mu VG$  trailing edge  
 $y$  = wall normal displacement  
 $z$  = spanwise displacement from tunnel centre-line  
 $z' = z/w$   
 $\delta$  = boundary-layer thickness based on  $0.99u_{fs}$   
 $\delta_i^*$  = incompressible boundary-layer displacement thickness  
 $\theta_i^*$  = incompressible boundary-layer momentum thickness  
 $\rho$  = time-averaged density  
 $\rho_{fs}$  = time-averaged freestream density  
 $\rho_w$  = time-averaged wall density  
 $\tau_w$  = time-averaged wall-shear-stress

### Subscripts

- 1 = station 1, upstream of the normal shock-wave  
2 = station 2, at the Pitot rake location

## I. Introduction

With the exception of the scramjet, all current air-breathing engine technology requires subsonic flow for combustion. This poses a particular problem in supersonic applications because of the requirement to decelerate the flow significantly before the engine. This is usually achieved using a system of oblique shock-waves, which are an efficient means of compression, followed by a terminal shock-wave within the inlet. Unfortunately, the interaction of these shock-waves with the inlet boundary-layers (shock-wave/boundary-layer interactions (SWBLI)) results in boundary-layer thickening and can trigger separation, both of which lead to large losses and distortion at the engine face.

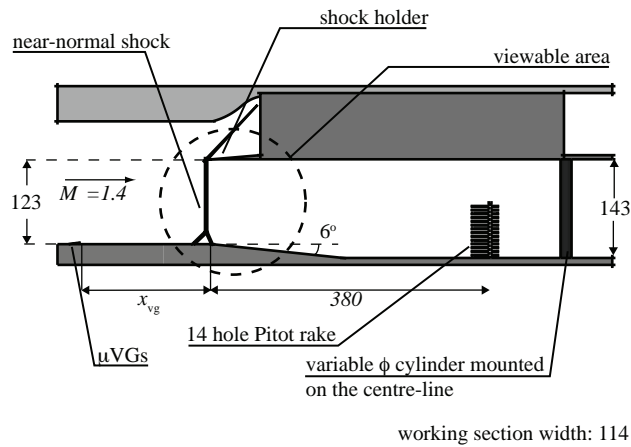
To avoid flow distortion and to maximize inlet pressure recovery, wall-suction or bleed is frequently employed to improve boundary-layer performance by removing low momentum fluid from the near-wall region via a number of holes, slots or scoops. Although effective, conventional bleed systems result in reduced mass flow to the engine, thereby reducing engine thrust. To compensate the engine inlet has to be larger, increasing weight and drag. Such a system also leads to a more complex inlet design, again increasing both weight and drag.

Recently, there has been a resurgence in interest in the use of vortex generators (VGs) to reduce separation in engine inlets.<sup>1-5</sup> These passive devices induce streamwise vortices which transfer high momentum fluid from the freestream to the boundary-layer, whilst simultaneously removing low momentum fluid from the near-wall region. Of specific interest are devices often referred to as micro-VGs ( $\mu$ VGs) or sub-boundary-layer VGs (SBVGs). These VGs, generally defined as those with heights less than a boundary-layer thickness, have been found to offer a similar level of mixing, but with a reduced drag penalty when compared to larger devices.<sup>6,7</sup> The main advantage of VGs over wall-suction is their simple and passive design which results in no decrease in mass flow to the engine. Their ability to be used alongside conventional bleed systems is also advantageous. However, before they can be introduced into the design of supersonic inlets, our understanding of these devices must be improved.

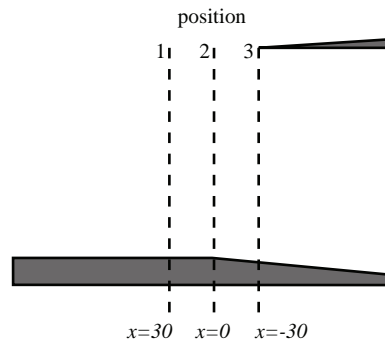
Until now, most studies of  $\mu$ VGs in SWBLIs have been performed in simple flow-fields, such as the flat plate normal or oblique SWBLI.<sup>1-4</sup> The flow in a real inlet, however, is considerably more complex. In particular, the boundary-layer is subjected to multiple shock-wave interactions and after the terminating shock-wave it also encounters a subsonic diffuser which imposes an additional adverse-pressure-gradient. Previous investigations on single shock-wave interactions alone (whether normal shock or oblique shock) do not provide information on the extent to which SWBLI flow control can alter the ability of the boundary-layer to deal with the subsequent diffuser, or whether flow control capable of beneficially affecting a SWBLI can also improve the coupled shock/diffuser problem. The study reported here therefore combines the effects of a terminating shock-wave and a subsonic diffuser in order to address this problem, and thus address at least some of the additional complexity found in a realistic diffuser flow.

## II. Experimental Arrangement

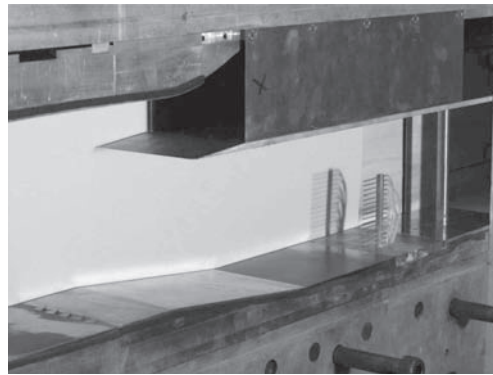
All experiments were undertaken in the blow-down type supersonic wind tunnels at the University of Cambridge. The setup within the working section is shown in fig. 1. The interaction of interest occurs below the shock holder, and is primarily contained within the area viewable through the tunnel windows. The incoming Mach number and the subsonic diffuser ramp angle were selected to approximate typical inlet flow conditions, and, on the basis of a review of the available literature, Mach 1.4 and  $6^\circ$  were chosen as appropriate values. Typically, inlets with such parameters require extensive flow control to perform satisfactorily, and it is thought that this is therefore a suitable starting point for an assessment of the potential of novel control techniques. The use of a shock holder allows the position of the terminating shock-wave to be controlled more easily. The shock holder improves shock stability as it allows spillage over the upper-side of the holding plate.<sup>8</sup> In this configuration, the working section is split into two channels: a lower choked section; and an upper unchoked and supersonic section. Such a configuration eliminates the problem of large scale unsteadiness (or even unstart) that has been known to occur in similar uncontrolled flow-fields to this.<sup>7</sup>



(a) Wind tunnel schematic



(b) Shock holder positions relative to the diffuser entrance



(c) Photograph of experimental arrangement

**Figure 1. Wind tunnel setup (all dimensions in mm)**

For all experiments, the stagnation temperature of the tunnel was within the range  $290 \pm 5$  K, and the stagnation pressure was nominally set to 205 kPa. This results in a nominal Reynolds number of  $26 \times 10^6$   $m^{-1}$ , and the variations in stagnation temperature and pressure results in a maximum variation in Reynolds number of less than 5%. At such high Reynolds numbers these variations can be assumed to have a negligible effect on the flow.

Flow visualisation has been carried out using a two-mirror schlieren system, and the surface-flow has been visualised using a mixture of paraffin, titanium dioxide and oleic acid. Schlieren images were taken with a digital SLR at shutter speeds of 1/800 s. Surface and Pitot pressure were measured using pressure transducers mounted outside the tunnel. Wall-pressure distributions were also measured using a pressure sensitive paint (PSP) system consisting of an ultraviolet light source and an acrylic based paint containing a luminescent dye. The luminescent dye emits red light at an intensity related to its partial pressure allowing

the wall-pressure distribution to be calculated. The error in the PSP system is thought to be  $\pm 5\%$ . A rake of 14 Pitot probes was used to determine the stagnation pressure distribution downstream of the diffuser at the simulated engine face or aerodynamic interface plane (AIP) (see fig. 1). The Pitot rake spanned the vertical range  $5 \leq y \leq 70$  mm with a (constant) 5 mm resolution. The rake could be positioned at 7 spanwise locations,  $-48 \leq z \leq 48$  with a 16 mm resolution, allowing three-dimensional contour plots of the downstream flow to be produced. The experimental error in the pressure transducers for the surface and Pitot pressure measurements is of the order 1%. The absolute spatial accuracy of each Pitot probe is thought to be around 0.5 mm. However, the difference in wall-normal placement of the rake between runs is negligible, allowing comparisons to be made with confidence. The incoming flow was measured using Laser Doppler Anemometry (LDA), and the accuracy of the LDA system is in the range  $\pm 1 \text{ ms}^{-1}$ .

The setup was designed so that the position of the shock holder could be adjusted easily, and as such, three different shock positions were examined. The three positions are shown in fig. 1. Position one ( $x = 30$ ), position two ( $x = 0$ ) and position three ( $x = -30$ ). The position of the terminating shock-wave was controlled by varying the downstream area near the exit of the lower section, and the mass flow was regulated in this way using different diameter wall-normal cylinders positioned on the centre-line. Cylinders were required with diameters between 15 and 18 mm, and these cylinders were placed a minimum of 8 cylinder diameters downstream of the AIP, as to not significantly influence measurements at this plane.

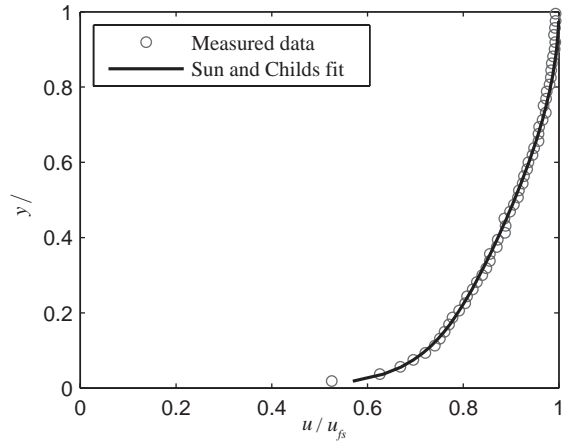
The near-normal shock-wave was located close to the lip of the shock holder by observing the schlieren image of the tunnel and adjusting the blockage accordingly. This typically led to an average shock-wave stand-off in the range 1-2 mm, giving a small amount of spillage over the top of the shock holder. By keeping the position of the terminating shock near constant throughout this investigation the VGs' ability to improve the flow-field through momentum transfer, and not through a modification to the shock position, can be ascertained.

### III. Characterisation of the incoming boundary-layer

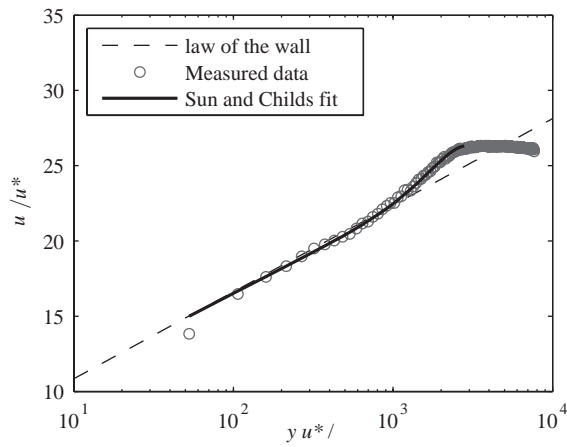
The incoming boundary-layer properties were measured using LDA. This data is shown in fig. 2, where the measured inflow boundary-layer profile is plotted alongside the generic turbulent boundary-layer fit proposed by Sun and Childs.<sup>9</sup> This plot, along with the wall-coordinate plot shown in fig. 2b, displays excellent agreement between the analytically derived profile and that obtained from measurements; demonstrating that the inflow boundary-layer closely resembles a fully developed zero-pressure-gradient turbulent boundary-layer.

Both the boundary-layer thickness and the value of the skin-friction coefficient was derived from this analytical fit. This data is shown in Table 1. The Reynolds number based on incoming incompressible displacement thickness ( $\delta_{i0}^*$ ) was found to be 14,000. The LDA derived velocity data also allows the boundary-layer characteristics and the appropriate scaling for the vortex generators with incoming boundary-layer thickness ( $\delta_0$ ) to be determined.

Assuming that the side-wall boundary-layers are approximately the same thickness as the tunnel-floor boundary-layer, a confinement parameter (here defined as the ratio of boundary-layer area to tunnel working-section area) was estimated to be around 2.5%.



(a) Mean velocity profile



(b) Mean velocity profile in log-law coordinates

$\delta_0$ (mm)	5.3
$\delta_{i0}^*$ (mm)	0.59
$H_{i0}$	1.35
$C_{f0}$	0.0021

Figure 2. Mach 1.4 incoming boundary-layer properties; LDA measurements and Sun and Childs fits shown

## IV. Uncontrolled interactions

Firstly, results are presented for the three baseline cases. Schlieren images for the three shock positions investigated are shown in fig. 3. Fig. 3a shows a schlieren image of the working section setup with the shock holder in position 1 ( $x = 30$  mm). The black area around the image indicates the edge of the schlieren mirror. The interaction regions for positions 1, 2, and 3 are shown in enlarged form in figs. 3b–d. The faint oblique Mach wave that can be seen in the bottom left-hand corner of the schlieren images is from the join between the diffuser and nozzle block. Its effect is negligible.

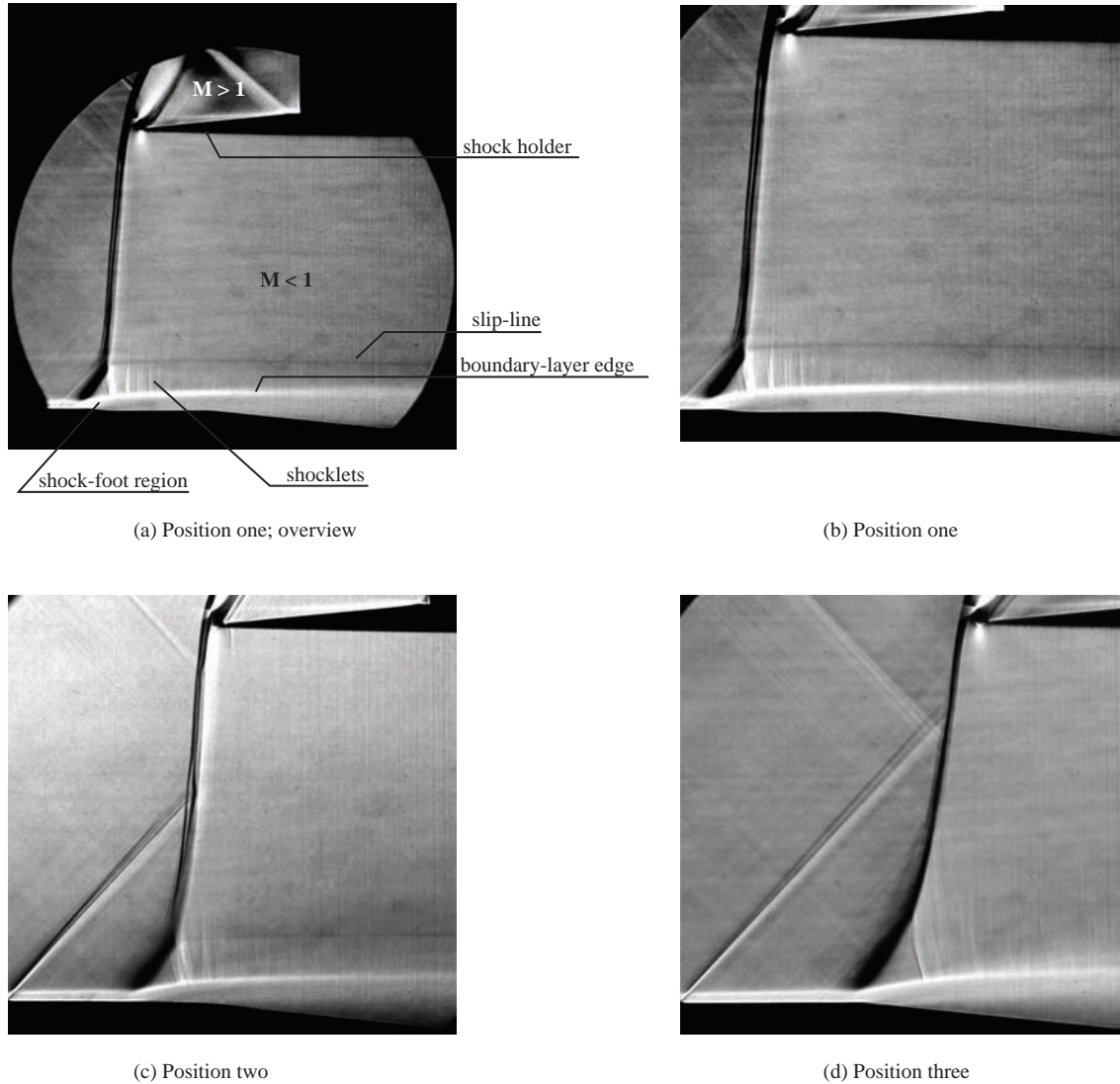


**Figure 3. Schlieren overviews (left) and close-ups (right) for each of the baseline interactions**

With the shock holder in position 1 ( $x = 30$  mm), the schlieren images (fig. 3a–b) illustrate a number of the features typical of a transonic SWBLI, and these features have been labelled for clarity in fig. 3a. The shock is bifurcated in the near-wall region, with the front leg emanating from the position where the boundary-layer starts to thicken, and this front-leg reaches the inviscid part of the shock at the triple point. The thickening of the boundary-layer continues through the interaction, with the boundary-layer only flattening off once it passes the rear leg of the shock, behind which there are a number of weak shocklets. This region of near sonic flow is often referred to as the supersonic tongue, and indicates re-acceleration of the near-wall flow because of the boundary-layer thickening. Once the boundary-layer enters the diffuser it is difficult to tell whether this layer remains attached or detaches, and as such, the viscous region from this point downstream is referred to as a shear-layer. The main body of the shock-wave stands close to vertical

just in-front of the lip of the shock holder; however, the slight shock curvature indicates that the shock is in fact a strong oblique solution of the Rankine-Hugoniot equations rather than a truly normal shock solution. This is a consequence of the non-uniform flow downstream of the shock-wave as a result of boundary-layer thickening and separation on the floor, and flow spillage ahead of the splitter plate.

When the shock-wave is moved downstream to position 2 ( $x = 0$ ) the shock structure looks similar, with a small increase in boundary-layer thickening across the interaction when compared to position 1. A much larger change in shock structure is observed when the shock holder is moved downstream to position 3 (see fig. 3d). In this figure there is a notable increase in the boundary-layer thickening across the interaction, which is also indicated by the movement of the triple point away from the wall. The main body of the shock is also more highly curved, especially in the region above the triple point. The boundary-layer also continues to thicken behind the rear-leg of the shock-wave, unlike before, and as such, at the edge of the image the shear layer/boundary layer is thicker than in positions 1 and 2. Although the shock holder is inside the diffuser, the strength of the shock-wave appears to not have increased as any expansion around the corner of the diffuser entrance is swallowed by the shock-foot.

Oilflow visualizations shown in fig. 4 reveal substantial changes to the near-wall flow as the shock is moved downstream, towards the diffuser. In position 1 the oilflow indicates that there is no large-scale separation along the tunnel centre-line—neither beneath the shock nor in the diffuser. Nevertheless, there is an area of low shear-stress beneath the shock, indicated by a whiter footprint in this region. The lack of shock-induced separation along the tunnel centre-line is in agreement with experiments conducted in this tunnel of a flat-plate transonic SWBLI.<sup>10</sup> As well as this, corner separations are visible, originating at the shock-foot location. These corner separations remain relatively small, like the flat-plate case, until the start of the diffuser where they start to expand again. The flow is also closely symmetric. This lack of shock-induced separation at this relatively high Mach number is discussed in detail by Burton et al<sup>11</sup> and is thought to be a result of three-dimensional effects. Agreement between the surface flow visualizations obtained in position 1 and in a configuration without a diffuser is evidence that the diffuser is too far downstream to have any significant detrimental effect in the interaction region itself.

In position 2 there is a marked change in the flow-field. Most visible in fig. 4b is the large change to the corner separations. It is evident that these side-wall interactions are strongly affected by the shock's position closer to the diffuser—large side-wall separations originate at the shock-foot. These structures grow quickly with streamwise distance and at their widest point cover more than half of the tunnel span. The flow in these corner separations seems to circulate around a central point. Again, there appears to be no shock-induced separation along the tunnel centre-line. Downstream of the shock-foot there is a large region of reversed flow in the diffuser, indicated by the almost two-dimensional separation line produced between the two corner interactions. The position of the separation line well downstream of the shock-foot suggests that the adverse-pressure-gradient of the diffuser is required on top of that of the shock-wave to cause detachment. The oilflow picture is also relatively symmetric with only a slight skew of the centre-line observed.

When the shock-wave is pushed further downstream the side-wall interactions are again very prominent, almost filling the whole tunnel span. These corner interactions also have clear foci, indicating that they wrap-up into vortices in this instance. The main difference to position 2 is that the centre-line flow now separates in the shock-foot location, which has been indicated in fig. 4. The flow is also very symmetric. The reattachment line for the centre-line flow is downstream of the diffuser, and at a similar location, for both positions 2 and 3.

Wall-pressure profiles of the centre-line flow measured using both pressure transducers and PSP are shown in fig. 5. It can be seen that there is generally good agreement between the PSP data and the pressure transducers. There is a small discrepancy at some streamwise locations when the shock holder is in position 1, and it is unclear as to why this is. In fig. 5b each of these profiles and a flat-plate Mach 1.4 wall-pressure profile have been superimposed on-top of one another so that the initial pressure rise starts at the same location. It can be seen that all the curves collapse to a single line in the first portion of the interaction. This agreement continues until the profile for position 3 starts to plateau, which occurs just at the start of the diffuser. This leveling off of the pressure-rise, and the plateau thereafter, are synonymous of separation. Downstream of the diffuser entrance, the pressure profiles for all three positions start to deviate significantly in response to the different distances between the shock-wave and diffuser.

It is apparent that in position 3 the flow is overcome by separation, and there is only a very slow increase in pressure in the diffuser, with the initial pressure in the diffuser lower than in the flat-plate case. This reduced pressure rise is likely to be due to separation observed in this case, which is not present in the flat-

plate case. The plateauing of the pressure-rise just inside the diffuser occurs at a pressure of approximately 0.49, which agrees well with the pressure level at separation predicted by the Free Interaction Concept.<sup>12,13</sup> By moving the shock upstream to position 2, it can be seen that the flow is able to diffuse significantly more than in position 3, although, the rise does flatten off in the diffuser as a result of the separation shown in the surface flow visualization. Moving the shock further upstream to position 1 results in further static pressure recovery than before. In position 1 the inflexion point at the entrance to the diffuser, suggests that the pressure rises from the SWBLI and diffuser have not fully merged (this inflexion is more easily observed by looking at the pressure transducer measurements). This response of the wall-pressure distribution to the diffuser entrance also indicates that the flow is attached here. When comparing the profile for position 1 with the flat-plate interaction profile, it can be seen that even upstream of the diffuser entrance the pressure is higher in position 1 than in the flat-plate case. The diffuser is undoubtedly influencing the flow upstream of its entrance. Again in position 1, the pressure rise flattens off in the second half of the diffuser, evidence that the thickening of the shear-layer at this point is approaching the rate of increasing area. There appears to be a clear advantage to placing the transonic SWBLI further upstream from the diffuser entrance: with each movement forward there is a linear improvement in normalized recovery of approximately 0.05.

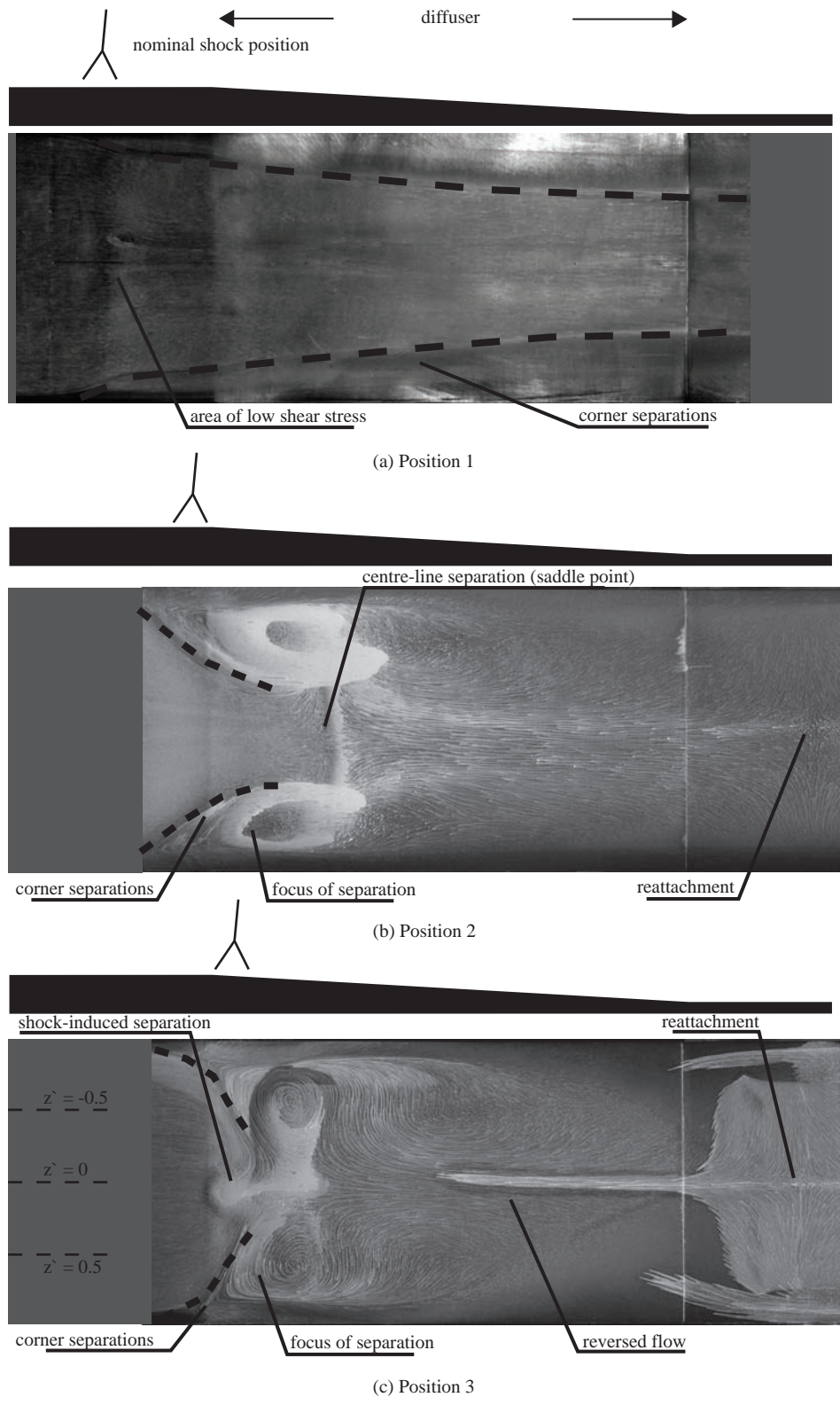
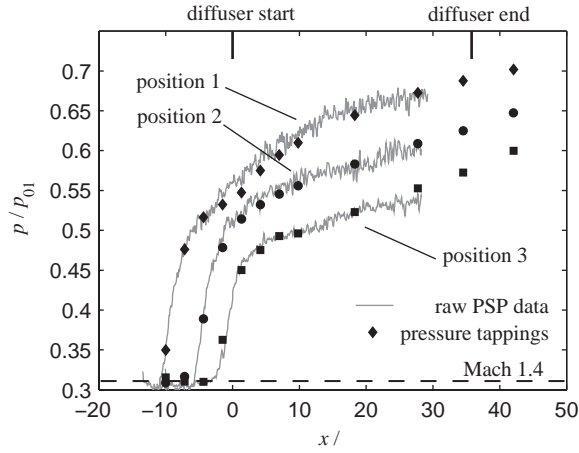
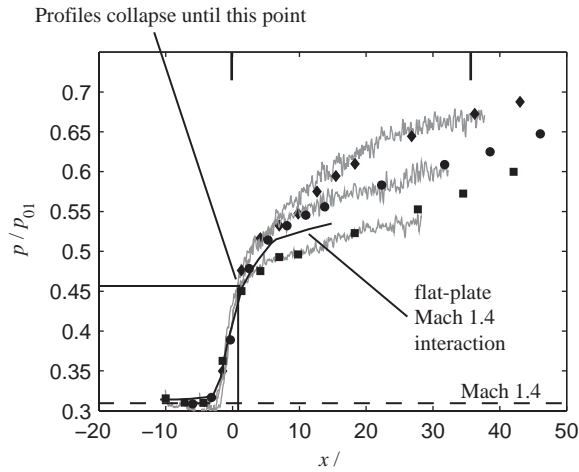


Figure 4. Oilflow for the three uncontrolled cases with the shock in position 1, 2 and 3 respectively



(a) Baseline wall-pressure profiles



(b) Baseline wall-pressure profiles with offset profiles

**Figure 5. Variation of wall-pressure throughout interaction and diffuser for the baseline cases**

These findings are in general agreement with the oilflow visualizations and Schlieren images. The centre-line wall-pressure profile for position 3 verifies that there is no expansion fan around the diffuser entrance: the wall-pressure profile already rising before this point. The wall-pressure fields for the three shock positions measured using PSP are shown qualitatively in fig. 6. The decrease in the overall pressure rise that occurs as the shock-foot moves downstream can be clearly seen from the slower transition from blue to red. What is clear from this figure, which was not apparent from the centre-line pressure profiles, is the increased three-dimensionality of the shock-foot region in the more downstream positions, and the pressure rise becomes increasingly more smeared near the side-walls. By comparing the oilflow images of fig 4 and these PSP images, it can be seen that the areas exhibiting shallower pressure rises match well with the location of the large corner separations. The presence of large corner separations therefore appears to inhibit the pressure rise introduced by the shock wave and diffuser as one might expect.

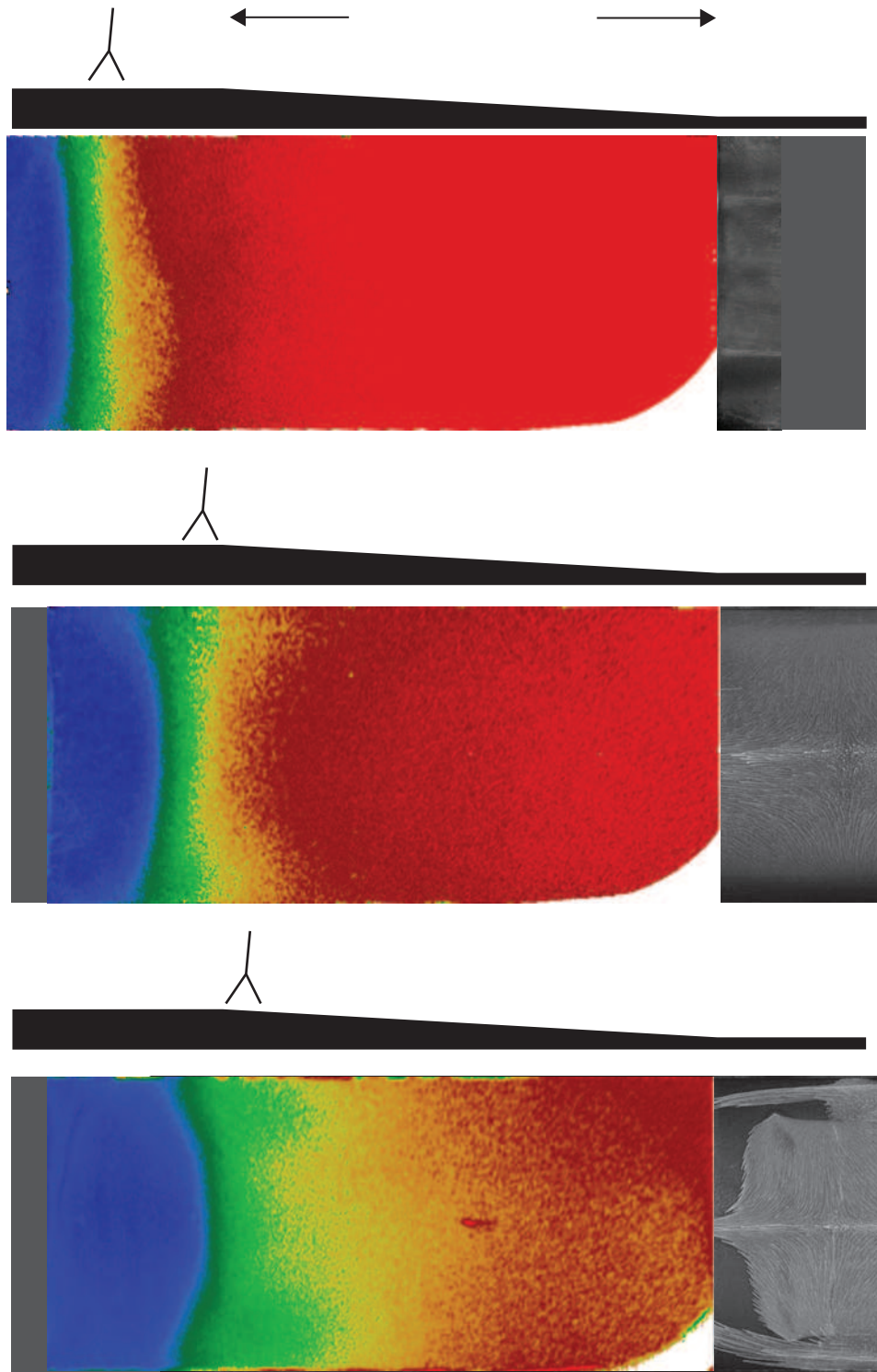


**Figure 6. Oilflow for the three uncontrolled cases with the shock in position 1, 2 and 3 respectively**

The total pressure measured at the AIP for each of the shock positions is shown in fig. 7. The lines bounding these plots on the left and right indicate the tunnel side-walls. Clear from these figures is a thickening of the shear-layer on the tunnel floor as the shock is moved downstream: this thickening shear-

layer resulting in the lower diffusion observed in the wall-pressure profiles. At the same time as this, the loss of total pressure also increases in the near-wall region—indicated by the darker regions close to the wall. This is more clearly shown in fig. 8 which shows the increase in losses along the tunnel centre-line as the shock is moved closer to the diffuser. The increase in pressure recovery in the outer region for position 3 is thought to be a result of the shock’s strong oblique behavior which results in lower entropy creation across the shock-wave.

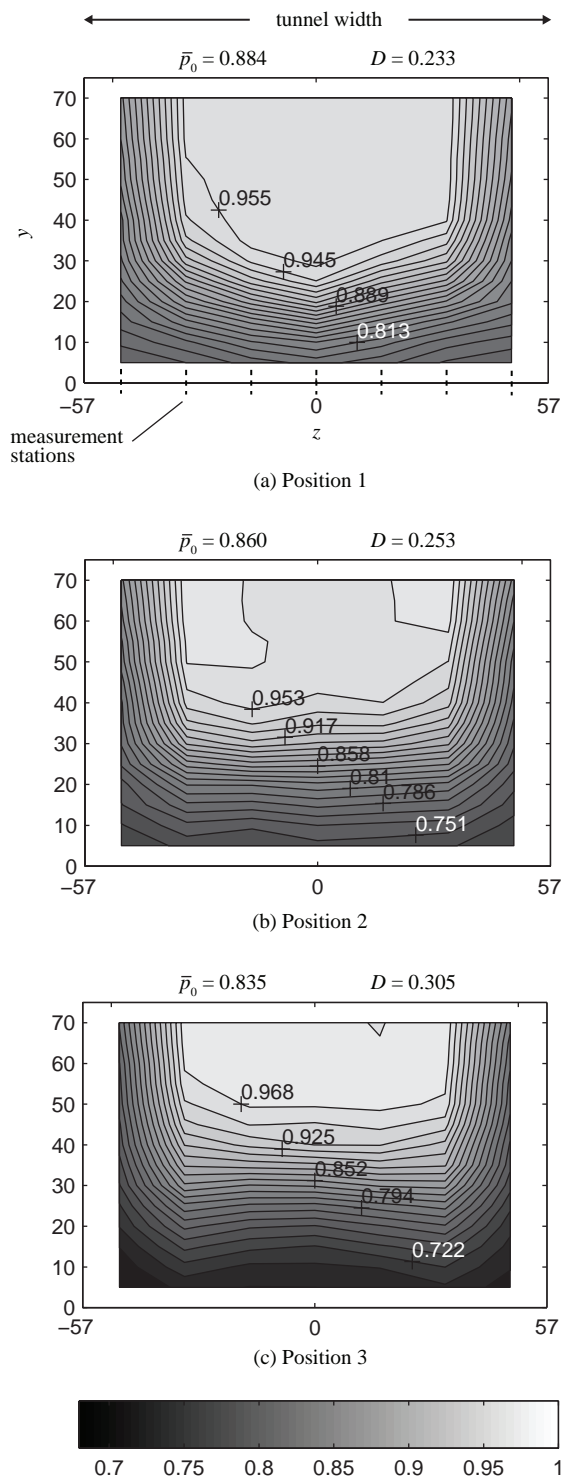
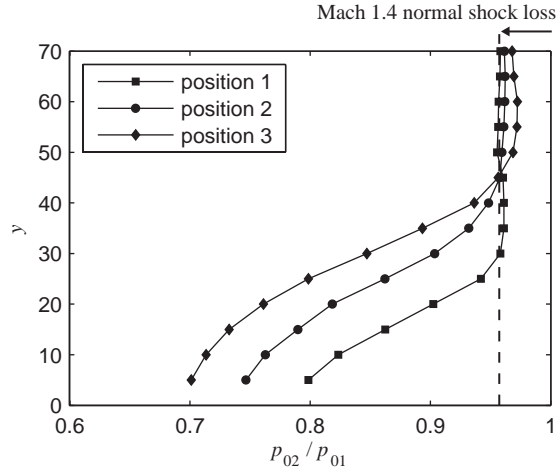


Figure 7. Total pressure profiles for the baseline cases, looking downstream. The dashed lines on the abscissa for position 1 indicate measurement locations

From fig. 7 a notable change to the variation of losses across the tunnel-span is also observed: the flow changes from having concave isobars in the near-wall region in position 1 to having convex curvature in position 3. The convex curvature in position 3 is thought to be caused by streamwise vortices, and these may be the same vortices that initiate from the foci of the corner interactions in fig. 4c. These streamwise vortices transfer higher total pressure flow from the outer flow towards the wall (see fig. 7c). Also indicated in these figures is the area-averaged total pressure and distortion, defined here as the maximum difference in total pressure, non-dimensionalized by the area-averaged total pressure. The average total pressure drops almost linearly at around 2.5% between shock positions, with the distortion rising slowly.



**Figure 8. Centre-line total pressure profiles for the shock in positions 1,2, and 3**

Between positions 1,2 and 3, little difference in the stagnation pressure profiles was measured when the rake was placed closest to the side-walls. Although the side-wall boundary-layers may be of similar extent at this location, the low resolution in this region makes it difficult to make conclusive observations about their extent and health (the Pitot rake only penetrates to approximately 50% of the side-wall boundary-layer thickness). The only indication of differences in side-wall behavior is seen through the spanwise variation of the tunnel floor flow.

These measurements show that there is a clear disadvantage to placing the shock too close to the diffuser. By placing the shock-wave right in the vicinity of the diffuser the boundary-layer immediately downstream of the shock has little, if any, time to recover before being subjected to a second adverse pressure gradient. From the data it is evident that the flow is highly sensitive to shock positioning close to the diffuser entrance. Only if the shock-induced pressure gradient and the diffuser pressure gradient are separated by a sufficient distance, allowing the boundary-layers time to recover, are relatively benign corner interactions observed. It is thought that by continuing to move the shock-wave upstream an optimal location may be found after which no further improvements to the downstream flow can be made. However, in these experiments such a location was not found. It is still unclear how the precise geometry in the vicinity of the shock effects the interaction and more work is required to obtain a better understanding of this flow. The difference in the flow-fields obtained in positions 1 and 2 indicates that the floor boundary-layer requires in the region of  $2\delta$  downstream of the shock-foot to recover before it can be subjected to another adverse-pressure-gradient without separating.

The significance of the side-wall interactions in each of the uncontrolled cases has resulted in a flow-field which differs somewhat from that which would be found in a typical inlet. In general, two-dimensional external compression type inlets are unlikely to have such substantial boundary-layers on three sides as is the case in these experiments, and as such, the corners would not be as dominant. Nevertheless, the corner interactions observed here would occur in similar flow-fields, but their relative importance depends on the aspect ratio and size (relative to the boundary-layer thickness) of the inlet duct.

## V. Vortex Generator Designs

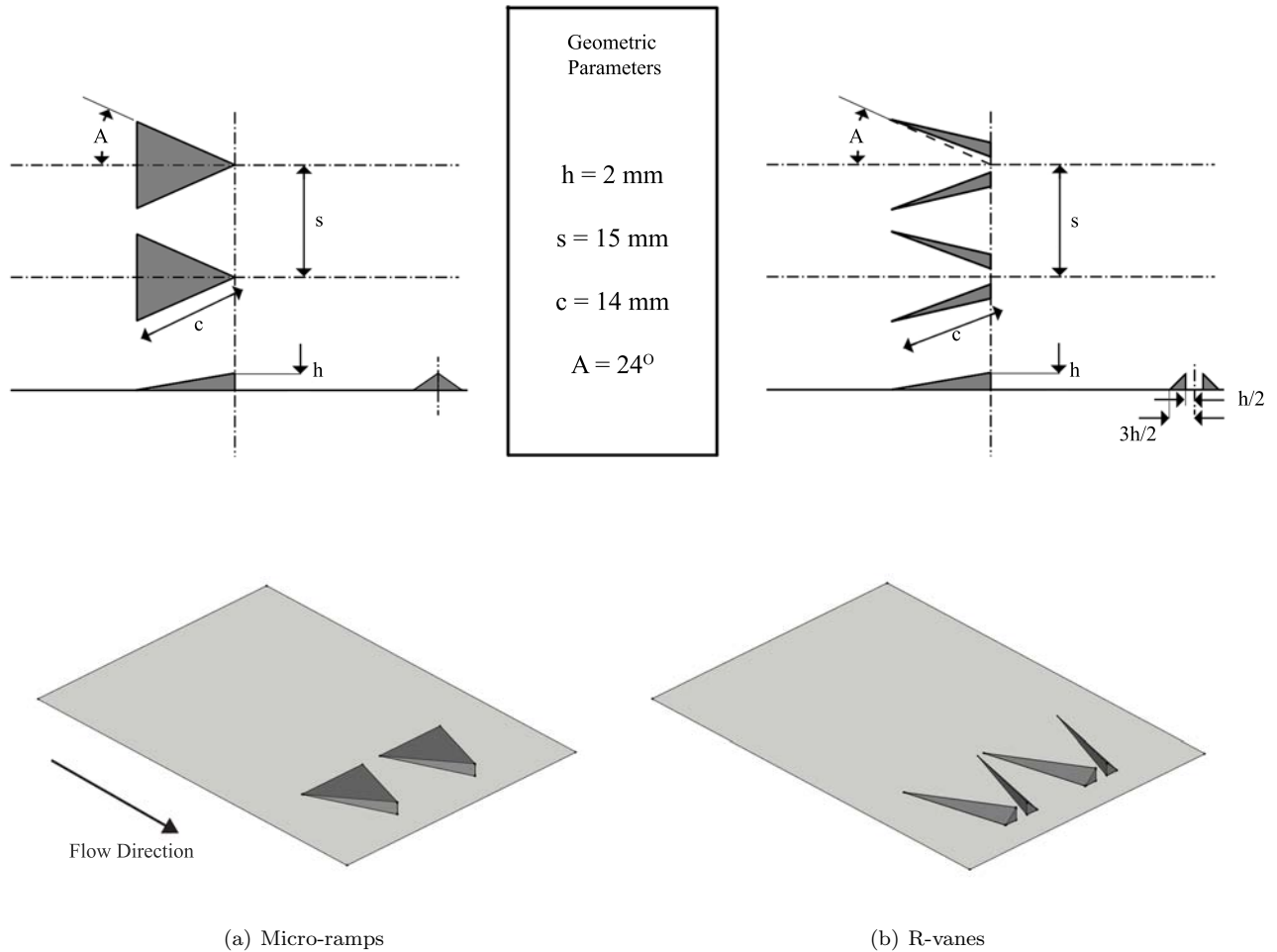


**Figure 9. Vortex Generator Geometries**

Two types of  $\mu$ VG were examined. The micro-ramp which has up until now been the most extensively used  $\mu$ VG in the literature,<sup>1-5</sup> and a new type of  $\mu$ VG, the robust-vane (r-vane), designed in-house. The geometries of the two  $\mu$ VG configurations are shown in fig. 9. The new type of VG tested here, the r-vane, is expected to provide a good compromise between vorticity generation and physical robustness. Compared to a standard vane-type VG there is significantly more contact area for fixation to the inlet walls and lower susceptibility to bending or accidental damage, much like the micro-ramp. Yet, a recent experimental investigation has suggested that the r-vane may produce enhanced levels of mixing when compared to the micro-ramp.<sup>14</sup>

The baseline flow has revealed extensive separation along the floor and in the corners. Ideally, flow control would address both of these problem areas, however, previous research has shown that the placement of  $\mu$ VGs ahead of corner flow regions has been detrimental, i.e., leading to large increases in corner separation.<sup>15</sup> On the other hand,  $\mu$ VGs have shown potential for controlling separations observed away from corners, such as seen here on the floor of the working section in positions 2 and 3. Therefore,  $\mu$ VGs were positioned so that they did not interact with the incoming side-wall boundary-layer flows. Consequently, arrays were limited to five  $\mu$ VGs.  $\mu$ VGs were added upstream of the shock, and all arrays were placed symmetrically across the tunnel.

Micro-ramps and r-vanes were placed upstream of the shock with the shock holder in position 3. The non-dimensional height of both types of  $\mu$ VG with respect to the incoming boundary-layer thickness is  $h/\delta_0 = 0.38$ . The micro-ramps were tested at four positions upstream of the diffuser entrance:  $x_{VG} = 3 \text{ mm}$ ,

33 mm, 63 mm, and 93 mm. These values correspond to a distance upstream of the baseline separation normalized by device height ( $\Delta x/h$ ) of 5, 20, 35, and 50.

## VI. Flow Control Through the Use of Vortex Generators on the Centre-line

A Schlieren image of the interaction region with micro-ramps is shown in figure 10. The  $\mu$ VGs are visible in the bottom left hand corner. The two oblique shocks radiating from the micro-ramps are the result of boundary-layer thickening in the vicinity of the  $\mu$ VGs' leading and trailing edges. This leads to a thicker boundary-layer approaching the interaction when compared to the baseline case. Although, the oblique shocks from the  $\mu$ VGs are visible in the schlieren images far downstream—intersecting with the normal shock—by this time they are merely Mach-waves, and have virtually no effect on the near-normal shock. Compared to fig. 3 there is a less pronounced lambda shock structure and no distinct triple point. The viscous region downstream of the shock is also more blurred than before.

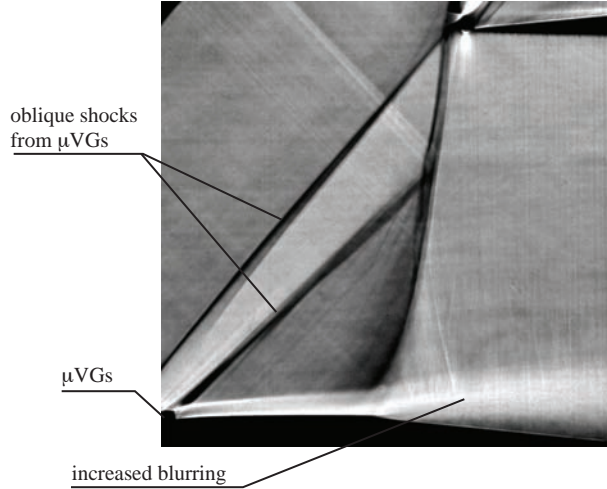


Figure 10. Schlieren image with micro-ramps at  $\Delta x/h = 35$

Surface oilflow visualizations with the micro-ramps are shown in fig. 11. From these pictures it is clear that the devices are not able to eliminate separation; however, in each case, a thin attached channel is achieved between the large recirculating separations on either side. These corner flows, again, originate near the nominal shock location, and are elongated when compared to before. At the same time, the reattachment line downstream of the diffuser has moved upstream when compared to the baseline case. These surface visualizations also suggest that the flow is relatively insensitive to  $\mu$ VG positioning; nevertheless, an optimum upstream distance at which the extent of the centre-line separation is minimized, was found to be  $\Delta x/h = 35$ .

To make a direct comparison with micro-ramps, r-vanes were tested at the optimal streamwise location for the micro-ramps. Some surface oilflow visualizations obtained with pairs of r-vanes are shown in fig. 12. A set of five pairs of r-vanes, which is directly comparable with the micro-ramps, is shown at the top of fig. 12. The resulting surface flow visualization exhibits very different features from that obtained with the micro-ramps. The most prominent feature is the highly asymmetric flow-field, with one corner interaction occupying around 75% of the tunnel span. At the same time, coupled with this, there is no separation along the central streamtube, which although highly skewed by the presence of the corner interactions, remains attached throughout the domain. This test case was repeated to eliminate the possibility that an air leak or an error in  $\mu$ VG placement was the cause of such asymmetry. The outcome of these tests was a near perfect reproduction of this flow-field. The r-vanes appear to influence the near-wall flow very significantly, and this is our first indication that r-vanes produce stronger vortices than the micro-ramps. When comparing the vortex footprints of the micro-ramps and r-vanes from the surface oilflow visualizations, it is difficult to obtain any conclusive evidence of the relative vortex strengths due to the small size of these devices.

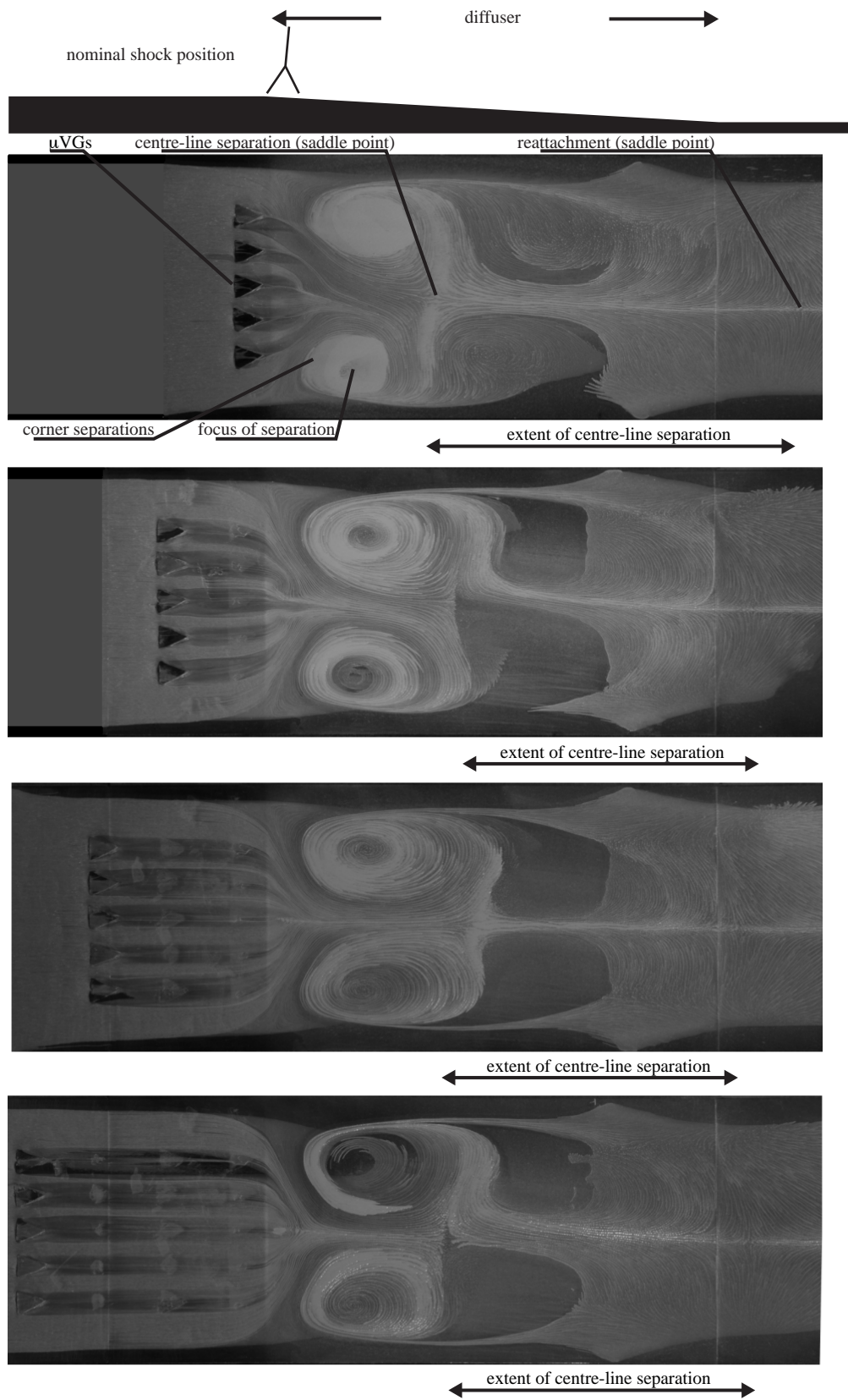


Figure 11. Micro-ramps placed at  $\Delta x/h$  equal to 5, 20, 35 and 50 respectively

A number of different r-vane arrays were tested to explore this phenomenon further, and surface flow visualizations for these are shown in fig. 12b-d. It is clear that as the number of pairs of r-vanes are reduced centre-line separation returns and flow symmetry is gradually restored. These findings suggest that the use of stronger flow control i.e. more pairs of r-vanes can lead to asymmetrical solutions. With only two pairs of r-vanes the flow-field looks relatively similar to that with five micro-ramps case, and there is a similar extent of attached flow between the two corner interactions (see fig. 12d). In the configuration the vortices from the r-vanes appear to be quickly swept towards the tunnel centre-line and this may therefore be why an attached channel between the two corners is produced in this case. As well as the asymmetry, it can be seen that in no configuration can a significant spanwise extent of attached flow be obtained. Also, in all cases the corner vortices are again enlarged by the presence of flow control on the tunnel-floor. The importance of the corner flows is compounded by the inability to obtain a symmetrical flow in many of the configurations.

These surface flow visualizations suggest that trying to energise the tunnel-floor leads to larger corner interactions, and in some cases with substantial energization near the centre-line, asymmetrical solutions can be obtained.

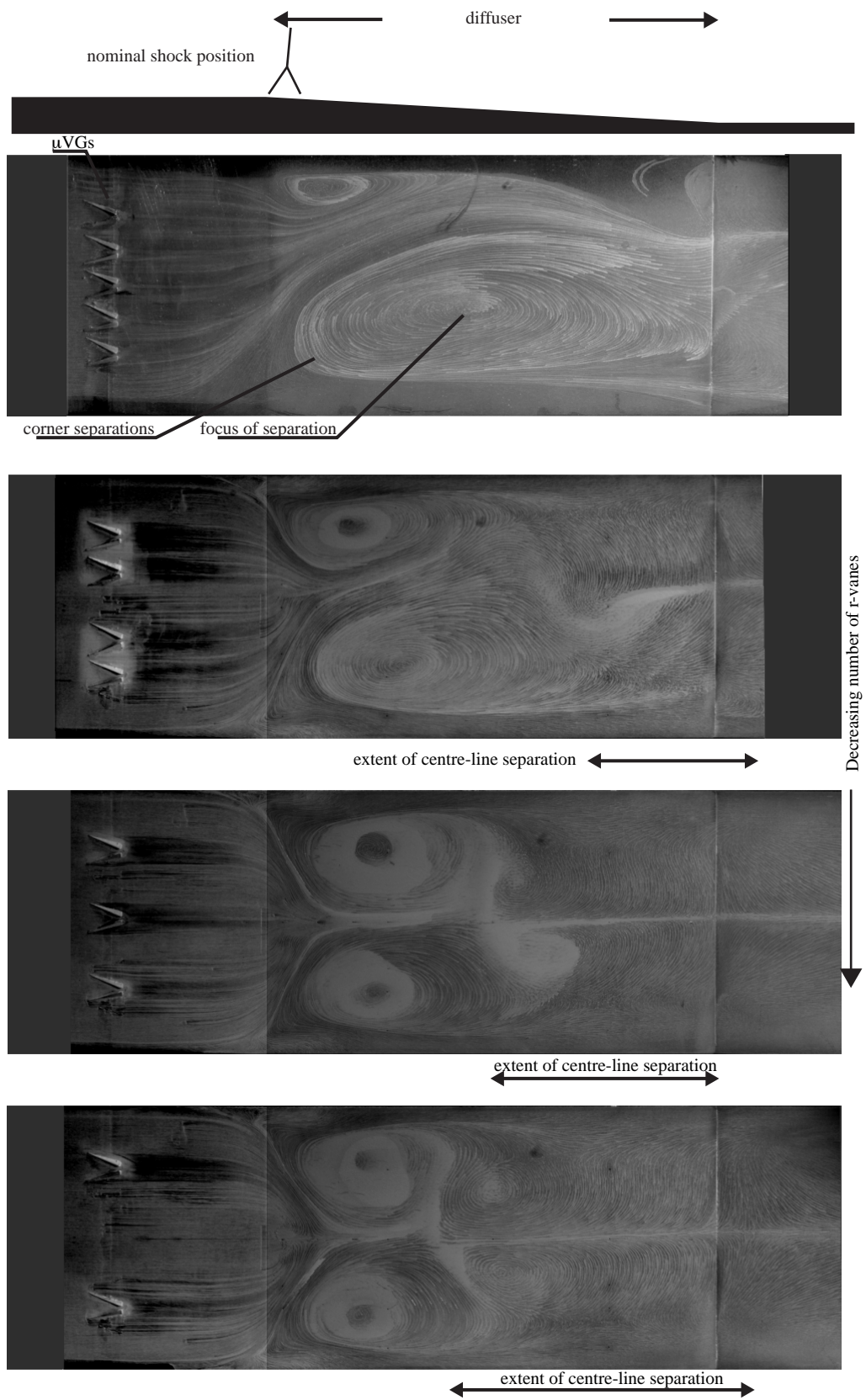
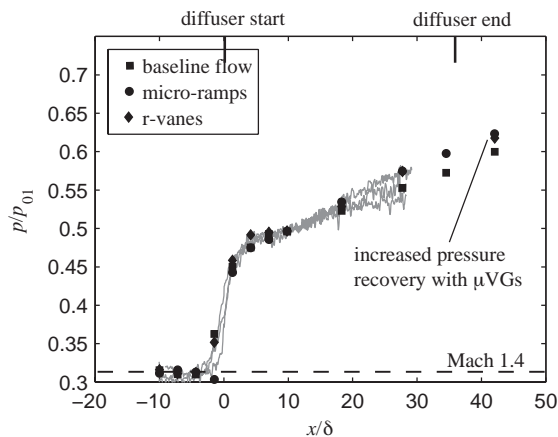
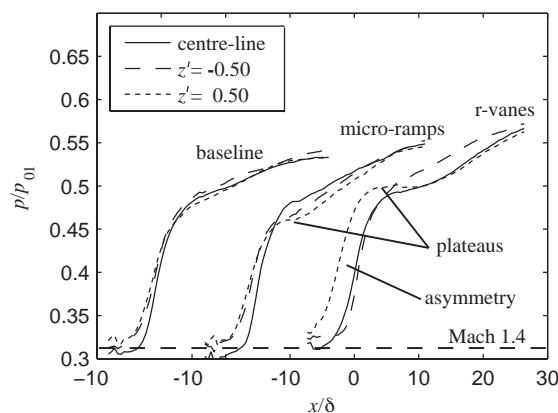


Figure 12. Arrays of five, four, three and two pairs of r-vanes

In fig. 14a the wall-pressure distributions with five micro-ramps and five pairs of r-vanes at  $\Delta x/h = 35$  are compared with the baseline case. One sees a small increase in the overall pressure rise with the addition of  $\mu$ VGs. However, all three profiles follow each other closely over the first half of the diffuser. In contrast, the behavior of the off-centre-line wall-pressure distributions vary somewhat between the three cases in the interaction region, as can be seen in fig. 14b (the spanwise locations of these off-centre-line distributions are shown in fig. 4c). These smoothed PSP measurements show a clear increase in the upstream influence distance away from the centre-line in the baseline case, after which both off-centre-line profiles follow the centre-line profile relatively closely. With the addition of the micro-ramps the off-centre-line pressure profiles plateau at a pressure significantly below the centre-line profile. This is probably due to the corner separations; nevertheless, by half-way down the diffuser the off-centre-line profiles rejoins the centre-line profile. In agreement with the surface-flow visualizations, a symmetrical flow is indicated by the minimal discrepancy between the two off-centre-line profiles for both the baseline case and the case with micro-ramps. With the inclusion of the five pairs of r-vanes, the off-centre-line wall-pressure distributions look somewhat different from the baseline and micro-ramp cases. Immediately obvious is the asymmetry, which is in good agreement with the surface-flow visualization. Both the  $z' = 0.50$  and the centre-line profile exhibit a prominent plateau which is a result of the very large corner separation covering both one-side and the centre-line flow. Whereas, the flow at  $z' = -0.50$  rises continually as this location is close to the location where the attached streamtube passes.



(a) Centre-line wall-pressure profiles for the baseline flow, micro-ramps, and r-vanes in position 3



(b) Span-wise variation of wall-pressure profiles for the baseline flow, micro-ramps, and r-vanes

**Figure 13. Wall-pressure variation with and without  $\mu$ VGs**

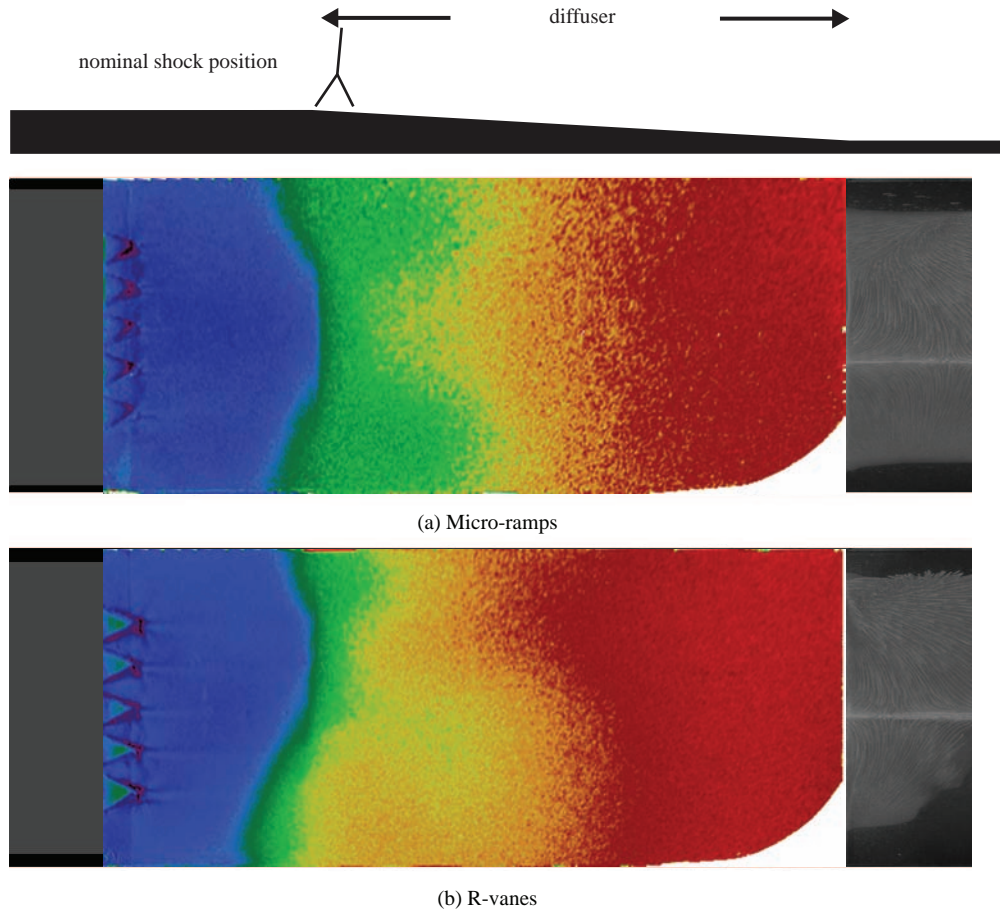


**Figure 14. Wall-pressure variation with and without  $\mu$ VGs**

One explanation for the increase in corner separations observed with flow control is that reduced separation along the centre of the tunnel increases the effective area change along the diffuser which in turn imposes a greater pressure gradient elsewhere. Since no flow control was employed along the side walls and in the corners this results in increased separation there—counteracting the beneficial effects seen along the floor. As a result, overall, there is little static pressure recovery change from the baseline case. Nevertheless, the central streamtube gains somewhat from a delayed separation, and the side-wall interactions loss out, with higher stagnation pressure loss in these regions. A similar conflict between the centre-line flow and side-wall flows have been observed by D. Burton et al<sup>11</sup> as well as by Bruce et al.<sup>16</sup> If the corners become so large that they are able to interact then this interaction may lead to the large-scale asymmetry.<sup>17</sup> Similar asymmetry to that observed in these experiments was obtained by Morris et al<sup>18</sup> with the use of boundary-layer control in the form of suction on the tunnel floor flow. In this case the side-wall were also left uncontrolled.

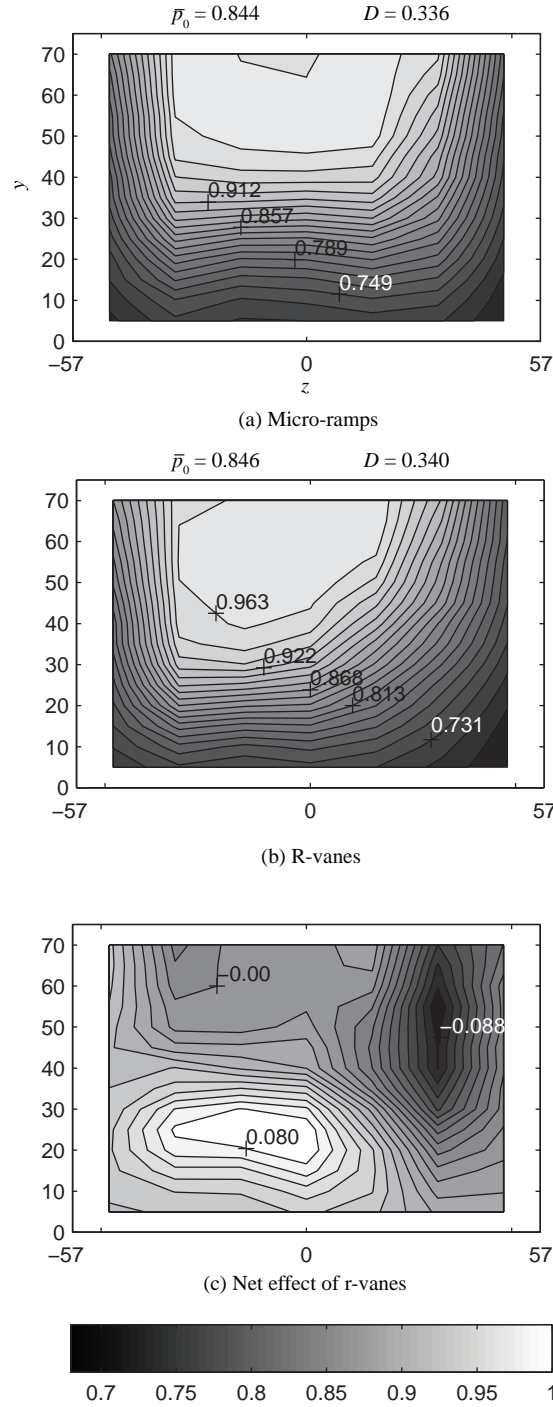


**Figure 15. Total pressure profiles (note that the colobar is not valid for (c))**

The total pressure profile at the AIP obtained with the five micro-ramps and the five pairs of r-vanes are shown in fig. 15. From these distributions it is clear that the  $\mu$ VGs have managed to reduce the stagnation pressure losses in the near-wall region. In the case of the micro-ramps, the region of loss is of a similar thickness to before, but the extent of the losses are partially reduced in the near-wall region. The average pressure recovery is increased by 1.5% and the distortion also rises from 0.305 to 0.336. The flow also appears reasonably symmetrical. The total pressure profile at the AIP with the inclusion of r-vanes is shown in fig. 15b. It can be seen that there is an improvement in the near-wall region at the location where the attached streamtube that passes between the side-wall interactions meets the rake. As expected there is

significant asymmetry and the large losses in the positive z side are apparent. Due to the detrimental effect the r-vanes have had on the side-walls the average pressure recovery remains practically unchanged (0.846 compared to 0.844) compared to the micro-ramps and the distortion is further increased. The r-vanes effect on the flow-field is emphasized in fig. 15c in which the change in total pressure between the baseline case and the case with the r-vanes is shown. Immediately clear is the improvement on the side where the central stream-tube is swept, and the high losses associated with the large corner interaction are also visible.

These results emphasize that to determine the potential benefits of different  $\mu$ VG configurations in more two-dimensional conditions typically found in engine inlets the corner interactions must first be controlled. At the same time, our fundamental understanding of these corner flows should also be improved due to their presence in a variety of applications. It is thought that the overall total pressure recovery can only be substantially improved if the corner flows and centre-line flow are both controlled.

## VII. Corner Bleed

One of the salient features of the investigation so far has been the high three-dimensionality that is introduced by the addition of the subsonic diffuser. Due to the low aspect ratio of the tunnel used, these separations are a very prominent feature of the flow-field. Alongside this, control in the form of VGs, have also enhanced the corner effects, and it was found that improvements along the centre-line were counteracted by increased losses in the corners and on the side-walls. Thus, it can be concluded that flow control of both the centre-line and corner flows is required.

As flow control in the corners using VGs has been shown previously to be unpredictable and often unfavorable,<sup>15</sup> in this investigation, control in the form of localized corner bleed is employed to reduce the prominence of the corner effects previously observed. By introducing corner bleed the difficulty of controlling the corner flows can also be determined. This in itself is important, as sharp corners such as those here may not be able to be avoided in certain inlet applications. Thus, understanding how best to control these flows is an important engineering consideration. Nonetheless, the main reason for introducing corner bleed is to try and provide a more two-dimensional flow-field. If a more two-dimensional separation can be obtained then this provides an improved baseline from which flow control relevant to a wider variety of supersonic inlet applications can be employed (not just those with prominent corner interactions, i.e., those with low aspect ratios).

The geometry of the suction slots is shown in fig. 16. The suction slots were connected to a vacuum pump, which can be run independently of the wind-tunnel. A standard orifice plate was used to regulate the suction mass flow. The back pressure in the suction system was adjusted such that the flow remained choked at the orifice plate throughout each tunnel run—resulting in constant mass flow through the slots.

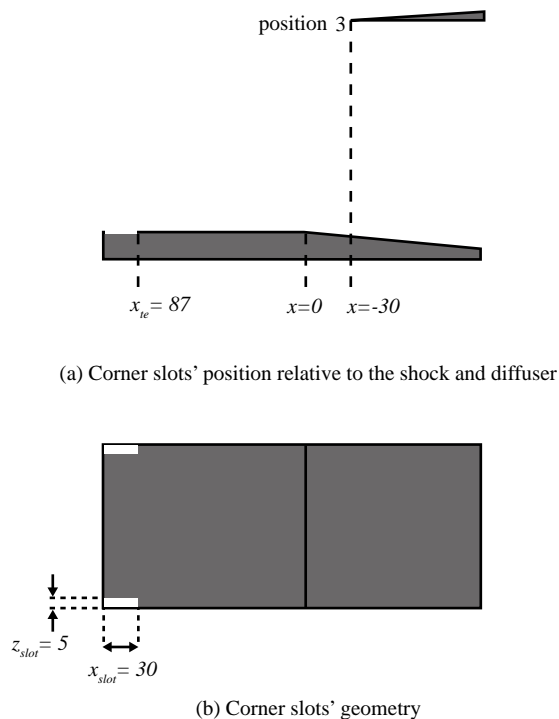


**Figure 16. Suction block details (all dimensions in mm)**

Throughout this investigation, the mass flow removed via the suction system was held constant. As a proportion of the tunnel mass flow ( $m_s/m$ ), the mass flow through the suction system was approximately 0.002, as a proportion of the mass flow passing under the shock holder ( $m_s/m_c$ ) approximately 0.003 and as a proportion of the tunnel-floor boundary-layer flow ( $m_s/m_{bl}$ ) around 7%.

## VIII. Control of Corner Interactions Using Corner Bleed

The schlieren and oilflow images of the flow in the presence of corner suction are shown in figs. 17 and 18 respectively. Comparing the schlieren images with and without suction (figs. 17 and 3), it can be seen that there is no clear difference between the two images. The fact that the schlieren image averages across the entire span may mean that any difference in the span-wise nature of the flow-field is obscured during this averaging process.

On the other hand, the oilflow image shown in fig. 18 displays significant differences to the baseline case. With the corner suction in place (the slots themselves can be seen near the far left of the figure, as indicated), there are a number of changes to the flow structure. Firstly, the separation line appears as a more two-dimensional line spanning the floor just downstream of the diffuser entrance. Within the diffuser itself, across a substantial part of the span, flow reversal now occurs in the stream-wise direction without interruption from the flow near the side-walls. Also, the flow near the side-walls now appears to be fundamentally different, with the reversed flow coming upstream to near the separation point before being entrained to either side. It therefore appears to be a secondary flow feature of the floor separation and not a separation resulting from the incoming boundary-layer in the corner itself.

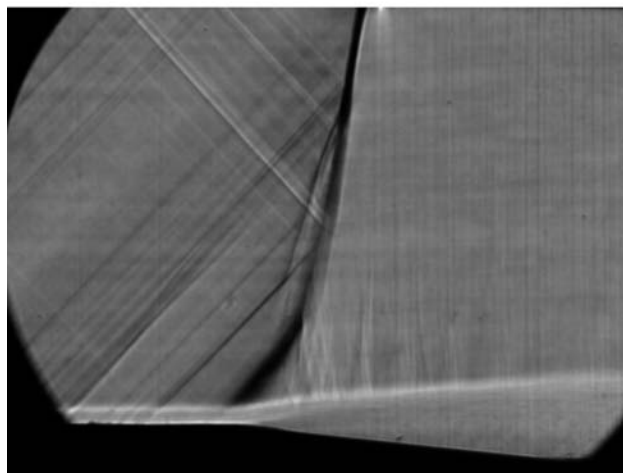


Figure 17. Schlieren image of the interaction region with corner suction

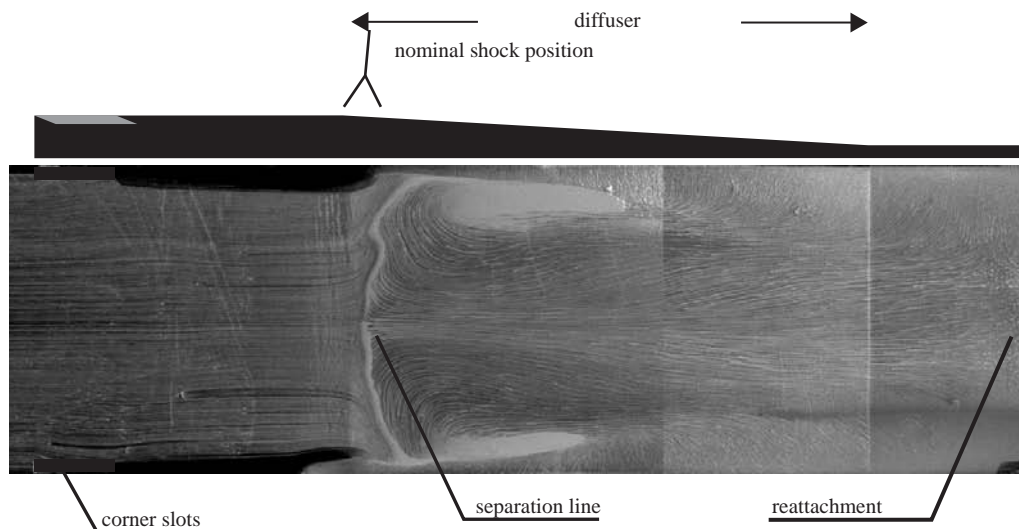


Figure 18. Arrays of five, four, three and two pairs of r-vanes

In fig. 19, the stagnation pressure profiles with and without suction at the AIP are shown for comparison. In general, it can be seen that the profiles with the slots present exhibit similar features to those without: the large losses at the wall are similar along the centre-line and off-centre-line; the side-wall profiles increase

approximately linearly with wall-normal distance.

A couple of subtle differences can be observed by looking more closely at the profiles. The most obvious difference is probably the near perfect symmetry observed in the suction case. This may be due to a damping out of imperfections in the inflow by the presence of the suction, a lower susceptibility to asymmetric effects without large corner interactions, or possibly better sealing of the tunnel on this occasion.

Looking at fig. 23 it is also visible that there is a slight reduction in the centre-line recovery with the suction in place, which indicates a stronger and more separated interaction in this region. Hence when control is applied to the corners, the centre-line flow actually sees a slightly detrimental impact on its recovery. This is, in fact, a similar phenomenon to that observed before in section VI. Instead of improving the centre-line and making the corner separations worse, in this instance the opposite effect has been observed whereby and improvement to corner region has actually made the centre-line separation worse. As a result, in both cases, although the flow topology differs significantly there is little overall impact on recovery. The slight improvement in overall pressure recovery is mainly due to improvements in the side-wall profiles. Again, control has had little impact overall, because it has not dealt with both aspects of the problem—the tunnel floor flow and the corner flows.

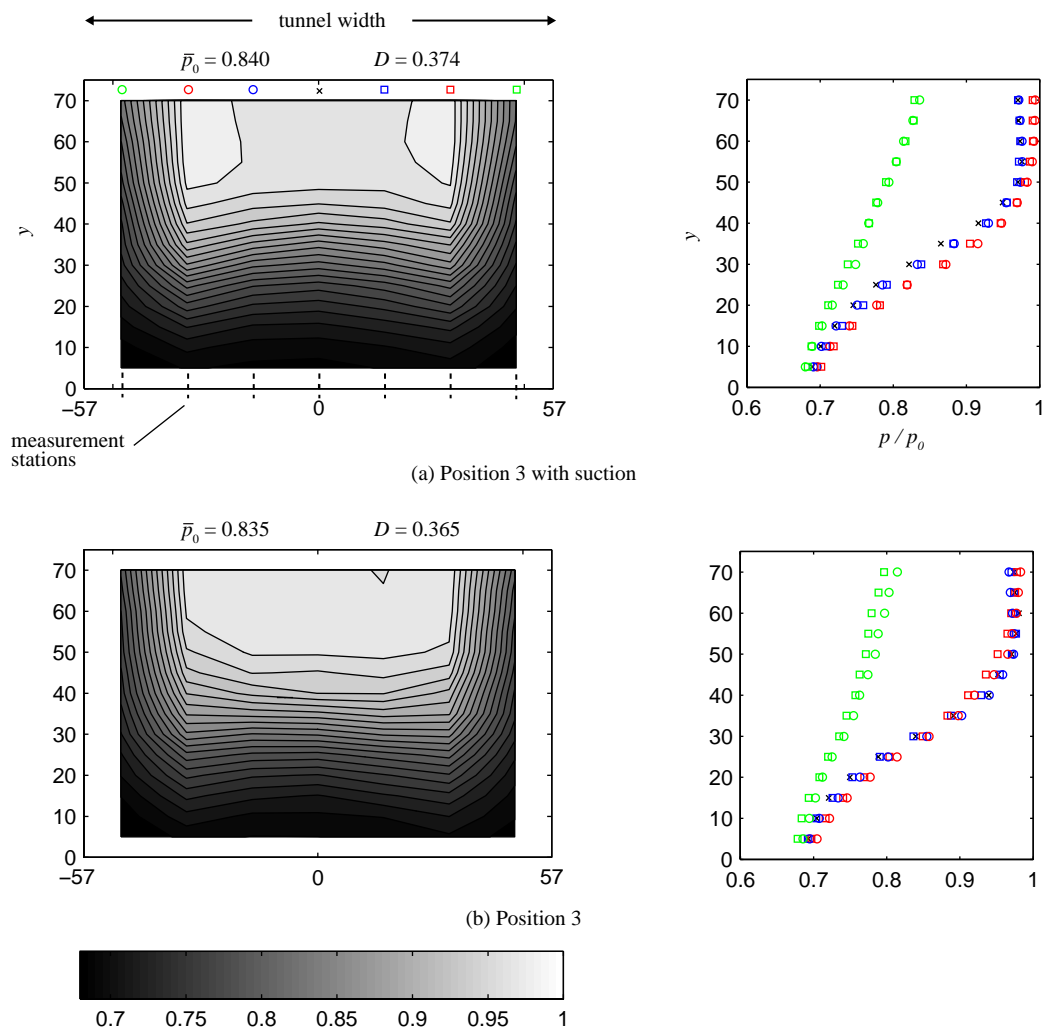


Figure 19. Comparison of total pressure profiles with and without corner suction

## IX. Flow Control Using both Vortex Generators and Corner Bleed

As the large corner separations initiated by the SWBLI and subsonic diffuser have now been significantly suppressed, flow control in the form of VGs was reemployed along the centre-line, but with the corner suction still in place, to try and reduce the extent of flow reversal within the diffuser. It was originally hoped that the previously used VGs and VG configurations could be repeated to give a direct comparison between the corner suction on and corner suction off cases. However, due to problems with the fabrication of the r-vanes, only micro-ramps were available for testing during the project timeframe.

The most favourable VG configuration for this flow-field actually turned out to be two rows of reversed micro-ramps. The schlieren image for this configuration is shown in fig. 20, and the VG configuration itself and the corresponding oilflow are shown in fig. 21. The first row of reversed micro-ramps consisted of five 2 mm ramps and the second row consisted of three 4 mm ramps. The most salient feature of this figure is the clear reduction in flow separation: through the entire diffuser there is channel of attached flow which occupies a large span-wise extent of the tunnel. Although small regions of corner separation has re-appeared near the entrance to the diffuser, these no longer occupy the large majority of the tunnel span. Even though the flow either side of the corner separations is predominantly attached, near the diffuser entrance there are small regions of reversed flow. These small patches of reversed flow occur in the upwash regions between each micro-ramp; the upwash of low momentum fluid between each VG then reduces the resilience of boundary-layer to separation in this region. Fully attached flow is obtained in each the the down-wash regions of the three large reversed micro-ramps. This breaking up of the separation into a more attached but also more three-dimensional flow has been observed in these tunnels previously but in the case of the oblique shock reflection.<sup>1</sup> In spite of the corner interactions being smaller, they still grow as the flow negotiates the diffuser, and by the end of the diffuser occupy close to a not insignificant 50% of the tunnel span. Once downstream of the diffuser, however, the corner interactions rapidly contract.

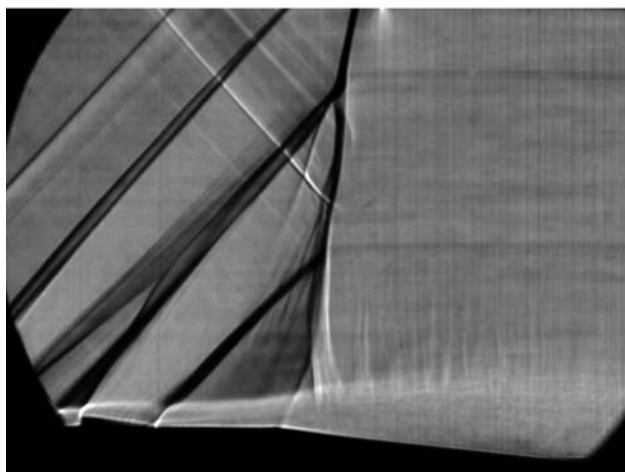


Figure 20. Schlieren image of the interaction region with corner suction and VGs

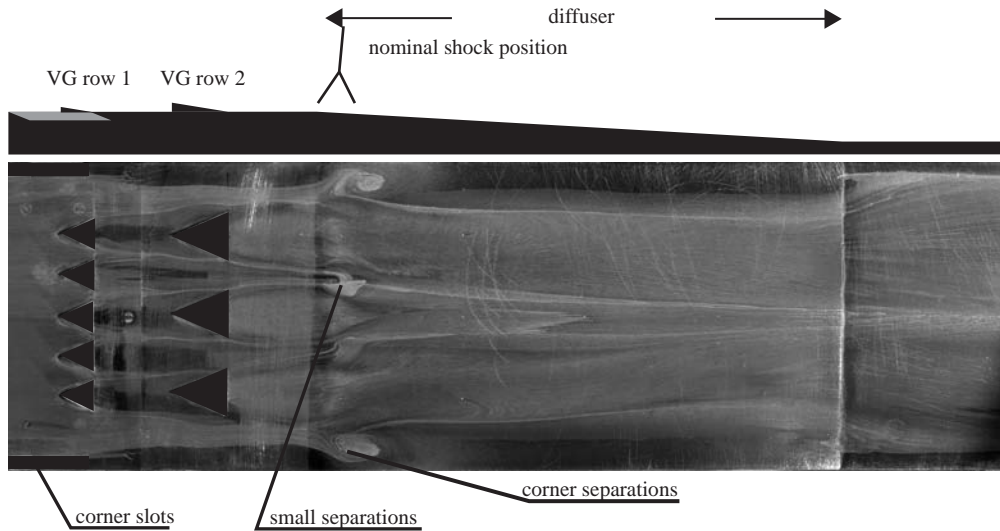
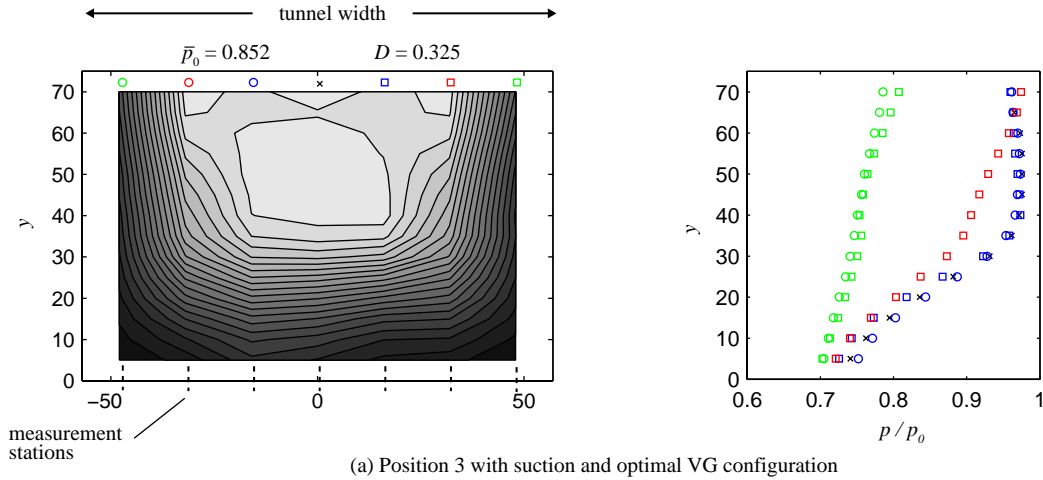


Figure 21. Oilflow of the configuration with both corner and VGs



(a) Position 3 with suction and optimal VG configuration

Figure 22. Total pressure profiles with both corner suction and VGs

Such a substantial reduction in flow separation with the use of micro-VGs has not, to the authors' knowledge, been previously documented. These findings are supported by measurements taken at the AIP (see fig. 22). Comparing the centre-line profiles with and without the VG configuration in fig. 23 reveals a noticeable improvement in the stagnation pressure in the near-wall region. Importantly, from fig. 22 it can also be seen that this same improvement is obtained at  $\pm 16$  and somewhat at  $+32$  (measurements were not obtained at  $-32$ ) showing that a significant span-wise extent of improved flow can be obtained. Unlike the thin channel of attached flow obtained in fig. 12. Unlike previously, there is also no real detrimental impact in the two side-walls, and the measurements at  $\pm 48$  look almost identical to those in the baseline case. As such, an improvement across the span of the tunnel has been gained for the first time without significant losses in either of the side-walls. However, with both the corner suction and VGs in place there is no net improvement in the side-wall profiles. As such, the lack of any improvement in the side-wall profiles and the detrimental impact on the flow at  $+32$  results, overall, in only a modest increase in pressure recovery from 83.5% to 85.2%. The reduction in distortion is more substantial with a drop from 0.365 to 0.325 observed in this instance.

These findings are also supported by the plot of the net total pressure difference between the baseline case and this VG configuration shown in fig. 24. It can be seen that there is an improvement across the entire span in the near-wall region, with only two small regions of higher loss at close to 50mm above the

surface.

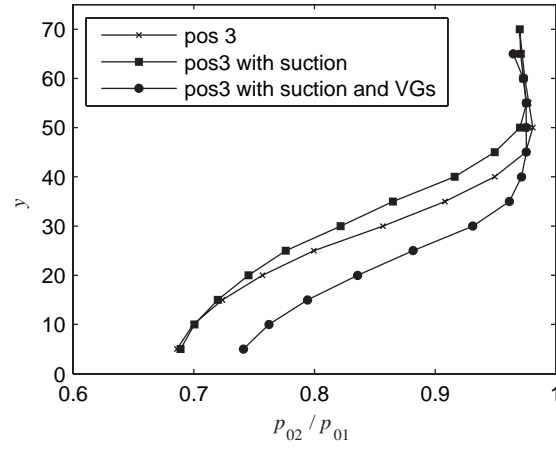


Figure 23. Comparison of total pressure along the centre-line for the baseline, suction and suction and VGs case

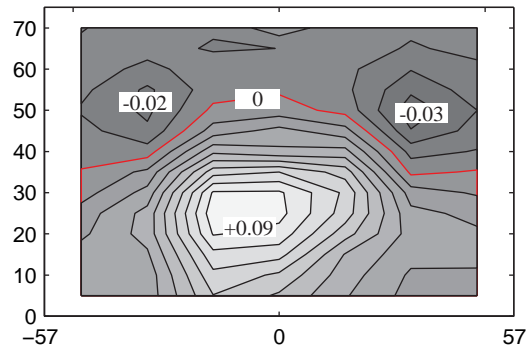


Figure 24. Net total pressure change from baseline with both corner suction and VGs

## X. Conclusions

The flow through a terminating near-normal shock-wave and a subsequent diffuser have been investigated. The conclusions of this study are as follows:

1.) When the near-normal shock-wave is placed far enough upstream of the diffuser attached flow is achieved along the centre-line, throughout the interaction and in the diffuser, and there are relatively small corner separations. As the shock-wave is moved closer to the diffuser, separation appears along the tunnel centre-line. Once a separated region exists, further downstream movement of the shock moves the centre-line separation point forward to beneath the shock-foot, even though no increase in the upstream Mach number is observed. As the shock-wave is moved downstream lower pressure recovery (both total and static) is observed and distortion is increased. It is clear that the diffuser has a strong influence on the flow when placed in the close vicinity of the SWBLI.

2.) As well as inducing centre-line separation, moving the shock-wave downstream also significantly increases the size of the corner separations, with a highly three-dimensional flow-field observed in position 3. Moreover, the influence of the corner flows is somewhat exaggerated by the relatively narrow tunnel working section, and in a real inlet, these flows would be less prominent. Nevertheless, corner flows are an important phenomenon which are, as yet, not fully understood

3.) Micro-ramps and r-vanes alone were able to partially remove separation from the centre-line and this resulted in higher total pressure recovery in the near-wall region at the AIP. At the same time as suppressing centre-line separation, both micro-ramps and r-vanes tended to enlarge and elongate the corner structures. As a result, the increase in both average total pressure and static pressure was confined to a limited area away from corner effects, and overall, integral improvements were small. This enlargement of the corner interactions is thought to be caused by the tunnel centre-line flow trying to induce a stronger pressure rise in the diffuser

4.) In some configurations, the application of VGs on the centre-line caused the flow to become asymmetrical, though the reasons for this are not yet known. A possible interaction between the two corners may be the cause of asymmetry

5.) The beneficial effects of flow control are to a great extent eradicated by a significant increase in the size and severity of corner separations. This highlights that any application of flow control in an inlet-relevant flow-field must address both, the sidewall/floor boundary layer interactions and the corner flow problem.

6.) When control was applied in the corners via traditional boundary-layer suction, a fundamental change in the separated flow topology was observed. The separation region which had been previously initiated by detachment in the corners was replaced by a more two-dimensional separation on the tunnel floor, and as a result, the extent of separation on the tunnel floor remained relatively unchanged. For such a change only a small bleed flow rate, approximately 0.3% of the mass flow under the shock holder, was required.

7.) Only when control of both the centre-line and corner flows was implemented could the extent of separation be reduced, and a relatively wide attached channel was produced in the diffuser. In this configuration a sizable improvement in pressure recovery was observed in the near wall region without a detrimental impact on the corner flows.

## XI. Publications

The following publications accompany this research project:

- Titchener, N. and Babinsky, H., "Microvortex Generators Applied to Flowfield Containing a Normal Shock Wave and Diffuser," *AIAA Journal*, Vol. 48, No. 5, May 2011, pp. 1046-1056.
- Bruce, P. K. J., Burton, D. M. F., Titchener, N. A., and Babinsky, H., "Corner effects and separation in transonic channel flows," *Journal of Fluid Mechanics*.
- Titchener, N. and Babinsky, H., "Microvortex Generators Applied to Flowfield Containing a Normal Shock Wave and Diffuser," 48th AIAA Aerospace Sciences Meeting and Exhibit, AIAA Paper 2010-0590, 2010.
- Titchener, N., Bruce, P., and Babinsky, H., "An Experimental Investigation of Corner Bleed Applied to a Normal Shock-Wave/Boundary-Layer Interaction and Diffuser," 49th AIAA Aerospace Sciences Meeting and Exhibit, AIAA Paper 2011-69, 2011.

## Acknowledgments

The authors would like to acknowledge the support of AFRL under grant number FA8655-08-1-3091.

## References

- <sup>1</sup>Babinsky, H., Li, Y., and Ford, C. W. P., "Microramp Control of Supersonic Oblique Shock-Wave/Boundary-Layer Interactions," *AIAA Journal*, Vol. 47, No. 3, March 2009, pp. 668–675.
- <sup>2</sup>Lee, S., Goettke, M., Loth, E., Tinapple, J., and Benek, J., "Microramps Upstream of an Oblique-Shock/Boundary-Layer Interaction," *AIAA Journal*, Vol. 48, No. 1, January 2010, pp. 104–118.
- <sup>3</sup>Ghosh, S., Choi, J., and Edwards, J., "Numerical Simulations of Effects of Micro Vortex Generators Using Immersed-Boundary Methods," *AIAA Journal*, Vol. 48, No. 1, January 2010, pp. 92–103.
- <sup>4</sup>Anderson, B. H., Tinapple, J., and Surber, L., "Optimal Control of Shock Wave Turbulent Boundary Layer Interactions Using Micro-Array Actuation," No. AIAA-2006-3197 in 3rd AIAA Flow Control Conference, June 5 - 8 2006.
- <sup>5</sup>Titchener, N. and Babinsky, H., "Micro-Vortex Generators Applied to a Flow-field Containing a Normal Shock-Wave and Diffuser," No. AIAA-2010-590 in 48th AIAA Aerospace Sciences Meeting and Exhibit, 2010.
- <sup>6</sup>Rao, D. and Kariya, T., "Boundary-layer submerged vortex-generators for turbulent flow separation control - an exploratory study," No. AIAA Paper 88-3546-CP, AIAA/ASME/SIAM/APS 1st National Fluid Dynamics Congress, Cincinnati, Ohio, July 25 - 28 1988.
- <sup>7</sup>Babinsky, H., Morgan, C., and Makinson, N., "Micro-Vortex Generator Flow Control for Supersonic Engine Inlets," No. AIAA 2007-521 in 45th AIAA Aerospace Sciences Meeting and Exhibit, Reno, Nevada, Jan. 8-11 2007.
- <sup>8</sup>Babinsky, H. and Ogawa, H., "Wind-Tunnel Setup for Investigation of Normal Shock Wave/Boundary-Layer Interaction Control," *AIAA Journal*, Vol. 44, No. 11 Technical Notes, November 2006, pp. 2803 – 2805.
- <sup>9</sup>Sun, C. and Childs, M., "A Modified Wall Wake Velocity Profile for Turbulent Compressible Boundary Layers," *Journal of Aircraft*, Vol. 10, 1973, pp. 381 – 383.
- <sup>10</sup>Bruce, P. and Babinsky, H., "An experimental study of transonic shock/boundary layer interactions subject to downstream pressure perturbations," *Aerospace Science and Technology*, Vol. 14, No. 2, 2010, pp. 134–142.
- <sup>11</sup>Burton, D., Bruce, P., and Babinsky, H., "Experimental Investigation into the Parameters Governing Corner Interactions for Transonic Shock-Wave / Boundary-Layer Interactions," No. AIAA 2010-0871 in 48th AIAA Aerospace Sciences Meeting and Exhibit, Orlando, FL, Jan. 4 - 7 2010.
- <sup>12</sup>Chapman, D. R., Kuehn, D. M., and Larson, H. K., "Investigation of separated flow in supersonic and subsonic streams with emphasis on the effect of transition," Technical Note 3869, NACA, Washington, 1957.
- <sup>13</sup>Erdos, J. and Pallone, A., "Shock/boundary-layer interaction and flow separation," *Heat Transfer and Fluid Mechanics Institute Proceedings*, 1962.
- <sup>14</sup>Li, Y., Internal report, Cambridge University.
- <sup>15</sup>Bruce, P., *Transonic Shock/Boundary Layer Interactions Subject to Downstream Perturbations*, Ph.D. thesis, University of Cambridge, Cambridge, UK, 2008.
- <sup>16</sup>Bruce, P., Burton, D., Titchener, N., and Babinsky, H., "Corner Flows and Separation in Transonic Channel Flows," 45th Symposium of Applied Aerodynamics, 3AF, Marseille, March 2010.
- <sup>17</sup>Bruce, P., Babinsky, H., Tartinville, B., and Hirsch, C., "Corner Effects and Asymmetry in Transonic Channel Flows," *AIAA Journal submitted Feb 2010 accepted June 2010*, 2010.
- <sup>18</sup>Morris, M. J., Sajben, M., and Kroutil, J. C., "Experimental Investigation of Normal-Shock/Turbulent-Boundary-Layer Interactions with and without Mass Removal," *AIAA Journal*, Vol. 30, No. 2, February 1992, pp. 359–366.